



3D *in vivo* Magnetic Particle Imaging of Human Stem Cell-Derived Islet Organoid Transplantation Using a Machine Learning Algorithm

Aixia Sun^{1,2†}, Hasaan Hayat^{1,3†}, Sihai Liu^{1,2,4}, Eliah Tull⁵, Jack Owen Bishop^{1,6}, Bennett Francis Dwan^{1,7}, Mithil Gudi^{1,3}, Nazanin Talebloo^{1,8}, James Raynard Dizon⁹, Wen Li^{10,11}, Jeffery Gaudet^{11,12}, Adam Alessio^{11,13}, Aitor Aguirre¹¹ and Ping Wang^{1,2*}

¹ Precision Health Program, Michigan State University, East Lansing, MI, United States, ² Department of Radiology, College of Human Medicine, Michigan State University, East Lansing, MI, United States, ³ Lyman Briggs College, Michigan State University, East Lansing, MI, United States, ⁴ Department of Orthopedics, Beijing Charity Hospital, Capital Medical University, Beijing, China, ⁵ Medgar Evers College, City University of New York, Brooklyn, NY, United States, ⁶ Department of Neuroscience, College of Natural Science, Michigan State University, East Lansing, MI, United States, ⁷ College of Natural Science, Michigan State University, East Lansing, MI, United States, ⁸ Department of Chemistry, College of Natural Science, Michigan State University, East Lansing, MI, United States, ⁹ Department of Radiology, UT Southwestern Medical Center, Dallas, TX, United States, ¹⁰ Department of Electrical and Computer Engineering, College of Engineering, Michigan State University, East Lansing, MI, United States, ¹¹ Institute for Quantitative Health Science and Engineering (IQ), Department of Biomedical Engineering, Michigan State University, East Lansing, MI, United States, ¹² Magnetic Insight Inc., Alameda, CA, United States, ¹³ Department of Computational Mathematics, Science and Engineering, College of Engineering, Michigan State University, East Lansing, MI, United States

OPEN ACCESS

Edited by:

Ming Li,
Osaka University, Japan

Reviewed by:

Aileen King,
King's College London,
United Kingdom
Luiza Ghila,
University of Bergen, Norway
Reihaneh Safaviohi,
Michigan State University,
United States

*Correspondence:

Ping Wang
wangpin4@msu.edu

† These authors have contributed
equally to this work and share first
authorship

Specialty section:

This article was submitted to
Stem Cell Research,
a section of the journal
Frontiers in Cell and Developmental
Biology

Received: 03 May 2021

Accepted: 15 July 2021

Published: 12 August 2021

Citation:

Sun A, Hayat H, Liu S, Tull E,
Bishop JO, Dwan BF, Gudi M,
Talebloo N, Dizon JR, Li W, Gaudet J,
Alessio A, Aguirre A and Wang P
(2021) 3D *in vivo* Magnetic Particle
Imaging of Human Stem Cell-Derived
Islet Organoid Transplantation Using
a Machine Learning Algorithm.
Front. Cell Dev. Biol. 9:704483.
doi: 10.3389/fcell.2021.704483

Stem cell-derived islet organoids constitute a promising treatment of type 1 diabetes. A major hurdle in the field is the lack of appropriate *in vivo* method to determine graft outcome. Here, we investigate the feasibility of *in vivo* tracking of transplanted stem cell-derived islet organoids using magnetic particle imaging (MPI) in a mouse model. Human induced pluripotent stem cells-L1 were differentiated to islet organoids and labeled with superparamagnetic iron oxide nanoparticles. The phantoms comprising of different numbers of labeled islet organoids were imaged using an MPI system. Labeled islet organoids were transplanted into NOD/scid mice under the left kidney capsule and were then scanned using 3D MPI at 1, 7, and 28 days post transplantation. Quantitative assessment of the islet organoids was performed using the *K-means++* algorithm analysis of 3D MPI. The left kidney was collected and processed for immunofluorescence staining of C-peptide and dextran. Islet organoids expressed islet cell markers including insulin and glucagon. Image analysis of labeled islet organoids phantoms revealed a direct linear correlation between the iron content and the number of islet organoids. The *K-means++* algorithm showed that during the course of the study the signal from labeled islet organoids under the left kidney capsule decreased. Immunofluorescence staining of the kidney sections showed the presence of islet organoid grafts as confirmed by double staining for dextran and C-peptide. This study demonstrates that MPI with machine learning algorithm analysis can monitor islet organoids grafts labeled with super-paramagnetic iron oxide nanoparticles and provide quantitative information of their presence *in vivo*.

Keywords: artificial intelligence, unsupervised machine learning, magnetic particle imaging, stem cell tracking, diabetes

INTRODUCTION

Type 1 diabetes (T1D) is characterized by an absolute deficiency of insulin secretion with hyperglycemia as a consequence. Transplantation of exogenous pancreatic islets to replace dead or dysfunctional endogenous beta cells is a strategy for controlling blood glucose levels in T1D patients. Severe shortage of cadaveric organ donors, requirement for lifelong immunosuppression, and reverting to using insulin after transplantation, however, largely hampers its application. In recent years advances in stem cell research, such as the derivation of human induced pluripotent stem cells (hiPSCs) and the emergence of organoid technologies, have enabled the creation of highly sophisticated human tissues and organ-like structures *in vitro*. These tissues could be used for isogenic or allogenic transplantation in the clinical setting to treat a diverse number of conditions, including T1D. *In vitro* created pancreatic islet organoids can be readily generated from hiPSCs matching the patient, thus providing an alternative similar to cadaveric donor islets that bypasses immune rejection concerns. Additionally, the number of pancreatic islet organoids that can be potentially produced is unlimited. A significant hurdle, however, is monitoring integration and survival of the pancreatic islet organoid after transplantation, and the lack of suitable non-invasive imaging techniques allowing us to determine the longer-term graft outcome (Rizzo et al., 2017; Wang and Aguirre, 2018).

Stem cell replacement therapy needs a technique that can quantitatively evaluate the fate of cells *in vivo* with high specificity and sensitivity. There are several techniques that have been used for imaging of islet or stem cell transplantation, including: optical imaging, magnetic resonance imaging (MRI) and positron emission tomography (PET). Optical imaging methods, both bioluminescence and fluorescence imaging, have the limitation of penetration depth preventing linear quantification and clinical translation. PET has excellent tracer sensitivity and depth penetration but cannot assess cell fate due to the limited tracer half-life. The evaluation of islet transplantation efficacy in the clinic relies on destructive analytical methods like histology or functional improvements that can take months to manifest. Most studies of cell tracking have used super-paramagnetic iron oxide nanoparticles (SPIONs) labeled cells, because SPIONs-based methods have few effects on cell viability, proliferation, and differentiation (Crabbe et al., 2010; Wang and Moore, 2012; Janowski et al., 2014; Bulte and Daldrup-Link, 2018), along with excellent depth penetration and *in vivo* persistence on the order of months. The primary challenge for MRI-based SPIONs cell tracking, however, is that SPIONs induced MRI signal dropouts that are difficult to distinguish from tissues with naturally low MRI signal (e.g., bones, tendon, lungs, bleeding, or any tissues near air). Moreover, MRI methods with positive contrast suffer from toxicity and sensitivity challenges (Magnitsky et al., 2017).

Magnetic particle imaging (MPI) is a novel imaging modality that directly detects the SPIONs, and is specific, sensitive, and linearly quantitative (Talebloo et al., 2020). MPI has been used for a wide range of biomedical applications such as tumors (Yu et al., 2017; Wu et al., 2019), vascular imaging (Khandhar et al., 2017), drug delivery (Wang et al., 2019), and *in vivo* tracking of labeled cells (Bulte et al., 2011; Zheng et al., 2015, 2016). Previously, our

group demonstrated MPI could be used for *in vivo* tracking of transplanted pancreatic islets in a mouse model (Wang et al., 2018). Furthermore, we have developed an unsupervised machine learning (ML) algorithm for monitoring *in vivo* 2D MPI data of islet grafts (Hayat et al., 2020). Such algorithms are required for standardized, high-throughput monitoring of transplanted organoids *in vivo* due to the highly variable nature of a region of interest (ROI) between MPI data. Often, it is difficult for human raters to maintain consistency regarding the threshold of cutoff for the true MPI signal from background. Therefore, applying a ML algorithm for segmenting of the desired ROIs from an MPI scan provides a reliable and standardized method of image quantification. So far, there are no reports on using MPI for imaging stem cell-derived islet organoids and it is critical to advance our algorithm to a 3D setting for more accurate and reliable signal quantification. Herein, we demonstrate the feasibility to develop and use the *K-means++* clustering-based, unsupervised ML algorithm to provide a novel method/tool for 3D image segmentation and quantification in the MPI domain, using SPIONs labeled stem cell differentiated islet organoids in a mouse model. We then used the segmentation output from the *K-means++* algorithm to generate a standard curve using fiducial markers in order to estimate the total iron value (TIV) of segmented ROIs. This provides information on the SPIONs accumulation within the labeled islet organoids and permits longitudinal evaluation of TIV of the ROI in the mice (Figure 1).

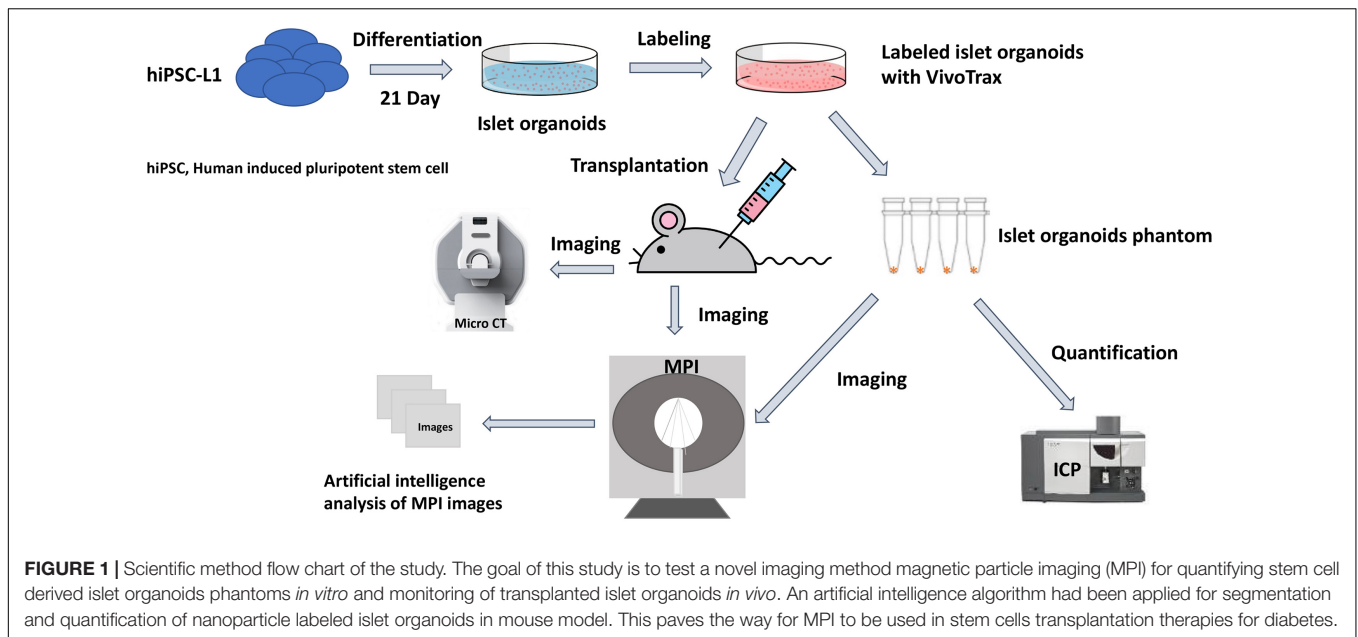
MATERIALS AND METHODS

Stem Cell Culture and Pancreatic Islet Organoid Differentiation

All hiPSC lines were validated for pluripotency and genomic integrity. hiPSC-L1 were cultured in Essential 8 Flex medium (Thermo Fisher Scientific, MA, United States) containing 1% penicillin/streptomycin (Gibco, Thermo Fisher Scientific, MA, United States) on six-well plates coated with growth factor-reduced Matrigel (Corning, NY, United States) in an incubator at 37°C, 5% CO₂, until 60–80% confluency was reached, at which point cells were split into new wells using ReLeSR passaging reagent (STEMCELL Technologies, Vancouver, BC, Canada).

To generate embryonic bodies, the confluent cultures were dissociated into small cluster suspension by incubation with accutase (Innovative Cell Technologies, Inc., San Diego, CA, United States). Cells were counted and each well of six-well low-adherence plates (Corning, NY, United States) were seeded with 5.5×10^6 cells in 5.5 ml Essential 8 Flex Medium supplemented with 10 ng/ml Activin A protein (Activin A, R&D Systems, MN, United States) and 10 ng/ml heregulin-beta-1 (PeproTech, NJ, United States). Plates were placed on an orbital shaker at 100 rpm to induce embryonic bodies.

To generate islet organoids, cell differentiation underwent five stages (21 days) was performed as described before (Russ et al., 2015). Briefly, to initiate differentiation, embryonic body was suspended into a low-adherence six-well plate in 5.5 ml d1 media [RPMI (Gibco) containing 0.2% FBS, 1:5,000 insulin-transferrin-selenium (ITS) supplement (Gibco), 100 ng/ml activin A, and



50 ng/ml WNT3a (R&D Systems)]. Media thereafter were changed daily, by removing either 4.5 ml media (at the end of d1) or 5.5 ml media the following days and adding back 5.5 ml fresh media until day 9. After day 9, only 5 ml of media was removed and added daily (Russ et al., 2015). Media in this differentiation protocol consist of the following: d2: RPMI containing 0.2% FBS, 1:2,000 ITS, and 100 ng/ml activin A; d3: RPMI containing 0.2% FBS, 1:1,000 ITS, 2.5 μ M TGF-beta Inhibitor IV (Calbiochem, MA, United States), and 25 ng/ml KGF (R&D Systems); d4–5: RPMI containing 0.4% FBS, 1:1,000 ITS, and 25 ng/ml KGF; d6–7: DMEM (Gibco) with 25 mM glucose containing 1:100 B27 (Gibco), 3 nM TTNBP (Sigma); d8: DMEM with 25 mM glucose containing 1:100 B27, 3 nM TTNBP, and 50 ng/ml EGF (R&D Systems); d9: DMEM with 25 mM glucose containing 1:100 B27, 50 ng/ml EGF, and 50 ng/ml KGF; d10–14: DMEM with 25 mM glucose containing 1:100 B27, 500 nM LDN–193189 (Stemgent, MD), 30 nM TPB (Millipore Sigma, MA, United States), 1,000 nM ALKi II (Axxora), and 25 ng/ml KGF; and d15–21: DMEM with 2.8 mM glucose containing 1:100 Glutamax (Gibco) and 1:100 non-essential amino acids solution (Gibco) (Russ et al., 2015).

Immunofluorescence Confocal Microscopy Imaging

Human islet organoids were transferred to microcentrifuge tubes (Eppendorf) using a cut 1000- μ L pipette tip to avoid disruption to the islet organoids and fixed in 4% paraformaldehyde solution for 15 min at room temperature. Fixation was followed by three washes in PBS and incubation in blocking solution (10% goat normal serum in PBS) on a thermal mixer (Thermo Scientific) at 300 RPM at 4°C overnight. Islet organoids were then incubated with anti-insulin primary antibody (Abcam, Cambridge, MA, United States) and anti-glucagon antibody (Abcam, Cambridge, MA, United States) in Antibody Solution

(10% goat normal serum and 0.5% bovine serum albumin in PBS) on a thermal mixer at 300 RPM at 4°C for 24 h. Primary antibody exposure was followed by three washes in PBS and incubation with FITC-labeled goat anti-mouse secondary IgG (Abcam, Cambridge, MA, United States) and Texas red conjugated goat anti-rabbit secondary IgG (Santa Cruz Biotechnology, Santa Cruz, CA, United States) in Antibody Solution on a thermal mixer at 300 RPM at room temperature for 1 h in the dark. The stained islet organoids were washed three times in PBS before being mounted on glass microscope slides (Fisher Scientific) using mounting medium containing DAPI (Vectashield; Vector Laboratories). Ninety micrometers Polybead Microspheres (Polysciences, Inc.) were placed between the slide and the coverslip (No. 1.5) to preserve some of the 3D structure of the organoids while accommodating the penetration capacity of the confocal microscope. Samples were imaged using an Olympus FluoView 1000 Filter-based laser scanning confocal microscope. Immunofluorescence images of islet organoids were semi-quantitatively analyzed using Fiji.¹ Briefly multi-color fluorescent images were split into single channels and converted to grayscale images. The area of interests was selected using selection tools in Fiji. The insulin and glucagon positive cells percentages of islet organoids were calculated.

Glucose-Stimulated Insulin Secretion Assay

One Hundred islet organoids (between 28 and 30 days of differentiation) were pre-incubated in 1 ml of low (2.8 mM) glucose Krebs buffer (KRB) and washed twice with KRB to remove residual insulin, then islet organoids were incubated in 1 ml of 2.8 mM glucose KRB for 30 min in a 37°C cell culture incubator, and the supernatant was collected. After they were

¹<https://imagej.net/Fiji>

washed twice with 2.8 mM glucose KRB, the islet organoids were incubated in 1 ml of high (28 mM) glucose Krebs buffer for 30 min, and the supernatant was collected. Human insulin was measured using the Insulin Human ELISA kit (Abcam, ab100578). Human insulin measurements were normalized by cell counts that were acquired by dispersing islet organoids into single cells with Accutase (Innovative Cell Technologies, Inc.) and counted using a cell counter.

Cell Labeling and *in vitro* Characterization of Labeled Cells

Islet organoids were feed with the concentration of 560 $\mu\text{g/ml}$ VivoTrax (Magnetic Insight Inc., Alameda, CA, United States) in CMRL media with 5% FBS and incubated for 48 h at 37°C with 5% CO₂ (Wang et al., 2018; Hayat et al., 2020). VivoTrax is a dextran coated SPION with core size of 4.2 nm and a mean hydrodynamic diameter of 62 nm. Cell labeling efficiency was tested using immunofluorescence staining for dextran coating with anti-dextran antibody (STEMCELL Technologies, Vancouver, BC, Canada), followed by an FITC-labeled goat anti-mouse secondary IgG (Abcam, Cambridge, MA, United States), mounted with a mounting medium containing DAPI and analyzed using fluorescence microscopy. Islet organoids viability was tested after labeling by colorimetric [3-(4,5-dimethylthiazol-2-yl)-2,5-diphenyltetrazolium bromide] assay according to the manufacturer's protocol (Promega, Madison, WI, United States) (Wang et al., 2011, 2012).

Cell function of secreted C-peptide was also tested using immunofluorescence staining with anti-C-peptide primary antibody (Abcam, Cambridge, MA, United States) and anti-dextran antibody (STEMCELL Technologies, Vancouver, BC, Canada), followed by an FITC-labeled goat anti-mouse secondary IgG (Abcam, Cambridge, MA, United States) and Texas red conjugated goat anti-rabbit secondary IgG (Santa Cruz Biotechnology, Santa Cruz, CA, United States).

Imaging of Islet Organoid Phantoms

In vitro phantoms comprising of different numbers of VivoTrax labeled islet organoids (0, 25, 50, 100, 200, and 400) in PBS were imaged using an MPI scanner (MOMENTUM MPI, Magnetic Insight Inc., Alameda, CA, United States) with the fiducial markers. Each 2D MPI images were acquired with parameters of a field-of-view (FOV) of 6 cm \times 12 cm, a 5.7 T/m selection field gradient, a drive field strength of 20 mT peak amplitude and a 45.0 kHz drive frequency. Images were reconstructed using x-space reconstruction. Quantification of the islet organoids phantoms was performed using the 2D MPI image intensity calibrated against a fiducial marker of known iron content (2.2 μg of iron) using VivoQuant imaging software (Invicro, Boston, MA, United States).

Inductively Coupled Plasma Optical Emission Spectroscopy

Iron content of labeled islet organoids were determined using inductively coupled plasma optical emission spectroscopy (ICP-OES). Different numbers of labeled islet organoids were digested

with concentrated nitric acid (Sigma-Aldrich, St. Louis, MO, United States). Digested samples were diluted and the total iron content of the samples were determined using an Agilent 710-ES ICP-OES (Agilent Technologies, Santa Clara, CA, United States). For the measurement of the iron content with ICP-OES, a calibration line was generated by six standard samples containing 0, 0.125, 0.25, 0.5, 1, 2, 3, and 4 ppm Fe. All iron standards were prepared from a stock certified standard reference material (FeCl₃, Iron Standard for ICP, 1000 \pm 2 mg/l Fe in 2% nitric acid, Sigma-Aldrich, St. Louis, MO, United States). An eight-point calibration curve was performed prior to sample analysis. The total iron content of samples was calculated, accounting for the number of islet organoids provided as well as dilution factors, as the mean value for analysis.

Cell Transplantation Under Kidney Capsule in a Mouse Model

All animal experiments were performed in compliance with institutional guidelines and were approved by the Institutional Animal Care and Use Committee (IACUC) at the Michigan State University. Labeled islet organoids were collected 1 h before transplantation. Female NOD/scid immunodeficient mice ($n = 5$, 10 weeks old, Jackson Laboratory, Bar Harbor, ME, United States) were anesthetized with 2% isoflurane. An incision made to expose the left kidney of the mouse, a catheter needle inserted underneath the kidney capsule and 800 islet organoids VivoTrax labeled were transplanted. Then the incision was closed, mice were monitored after transplantation.

MPI Tracking of Transplanted Islet Organoids Under Kidney Capsule of Mice

Under anesthesia with 2% isoflurane, mice were imaged using 3D MPI at 1, 7, and 28-day post-transplantation ($n = 3$) with operating parameters, a FOV of 6 cm \times 6 cm \times 12 cm, acquisition time of 10 s per projection (total 55 projections) plus 30 s for automatic set up of the magnets, with an approximate total time of 35 min including for image reconstruction. Anatomic CT reference images were acquired by the whole-body model of Perkin Elmer QuantumGX microCT. MPI images were co-registered to CT with fiducial markers using VivoQuant Imaging Software (Invicro, Boston, MA, United States). Control animals did not receive islet organoids ($n = 2$).

3D *K-means++* Unsupervised Machine Learning Algorithm

In order to segment the ROI from the MPI, we used the previously established *k-means++* algorithm for ROI segmentation and a standard curve model for prediction of the TIV of the cells (Hayat et al., 2020). This TIV correlates linearly to increasing ROI intensity and size (Hayat et al., 2020). Hence, here we apply the *k-means++* algorithm to a 3D MPI Image sequence through layer-by-layer segmentation of the individual ROIs and TIV estimations from 32 to 36 layers per scan, and these values are summed to provide a TIV for the entire 3D structure. As determined in our previous study by the elbow method, the *k*-value for number of centroids in this study

was 4 (Hayat et al., 2020). The concentrations of the fiducial markers (1 μ l) used to generate the standard curve were 10, 20, and 40% of VivoTrax solution (5.5 mg/ml iron). For all MPI image scans, placement of fiducial markers was kept in the same location in order to provide optimal data for *k-means++* segmentation of the ROI and subsequent TIV estimation *via* the generated standard curve.

Intraclass Correlation Coefficient Validation

In order to measure accuracy of the algorithm and determine its validity, its TIV prediction was compared to that of a manual rater, in this case a board-certified radiologist. The rater segmented the ROI manually on 15 images using the VivoQuant Imaging Software (Invicro, Boston, MA, United States), and total pixel sum values were extracted for TIV analysis from the ROIs using a ratio method with reference to a singular fiducial marker for TIV prediction (Makela et al., 2020), calibrated against a 40% fiducial marker of known iron concentration (2.2 μ g of iron). For statistical analysis, SPSS statistical software (IBM, Armonk, NY, United States) was used to calculate intraclass correlation coefficient (ICC), which provides a measure of the inter-rater reliability between the rater and algorithm. A two-way mixed model with a confidence interval of 95% was selected, and a measure of absolute agreement was calculated with the ICC. A higher ICC score indicates greater reliability of algorithm performance due to the high degree of agreement between the rater and algorithm.

Ex vivo Immunohistochemistry

After the last round of MPI, animals were sacrificed and left kidneys were removed, fixed in 4% paraformaldehyde solution for 16 h at 4°C, and embedded in paraffin. Paraffin sections of grafts under the left kidney capsule were incubated with anti-C-peptide primary antibody (Abcam, Cambridge, MA, United States) and anti-dextran antibody (STEMCELL Technologies, Vancouver, BC, Canada) at 4°C for 16 h, followed by an FITC-labeled goat anti-mouse secondary IgG (Abcam, Cambridge, MA, United States) and Texas red conjugated goat anti-rabbit secondary IgG (1:100 dilution, Santa Cruz Biotechnology, Santa Cruz, CA, United States) at room temperature for 1 h. All sections were mounted with a mounting medium containing DAPI (Vectashield; Vector Laboratories) and analyzed using fluorescence microscopy (Eclipse 50i; Nikon Metrology, Brighton, MI, United States) (Pomposelli et al., 2020; Wang et al., 2020).

Statistical Analysis

Data are presented as mean \pm SD. Statistical comparisons between two groups were evaluated by Student *t*-test and corrected by one-way ANOVA for multiple comparisons using GraphPad Prism 5 (GraphPad Software, Inc., La Jolla, CA, United States). A two-way repeated measures ANOVA was performed for evaluating TIV predictions as the independent variable for different imaging days. Correlation and linear regression analysis between measured iron content in the

phantoms and the number of labeled islets was assessed using GraphPad Prism 5 and SPSS statistical software (IBM, Armonk, NY, United States) as well. A value of $p < 0.05$ was considered to be statistically significant.

RESULTS

Characterization of Differentiated Islet Organoids

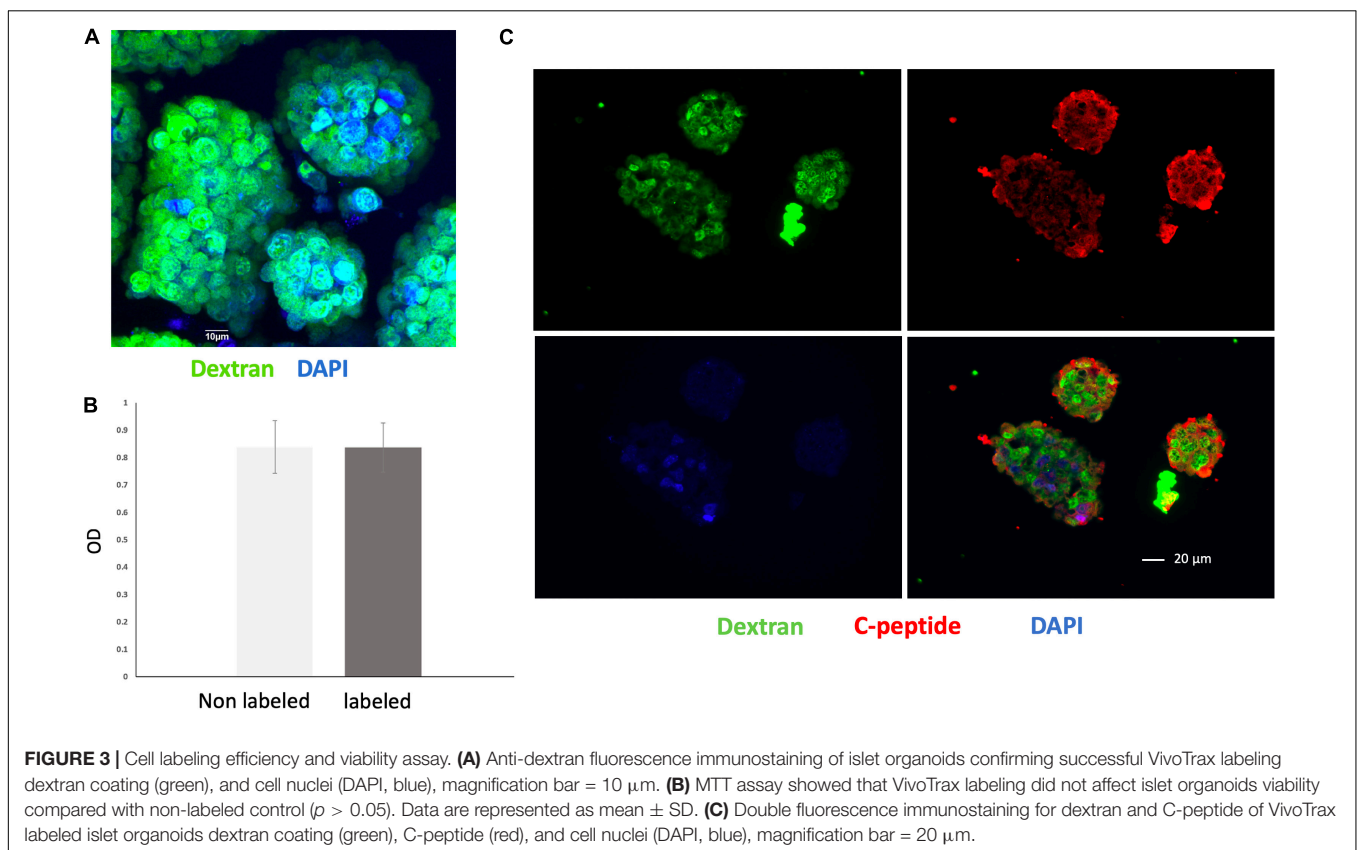
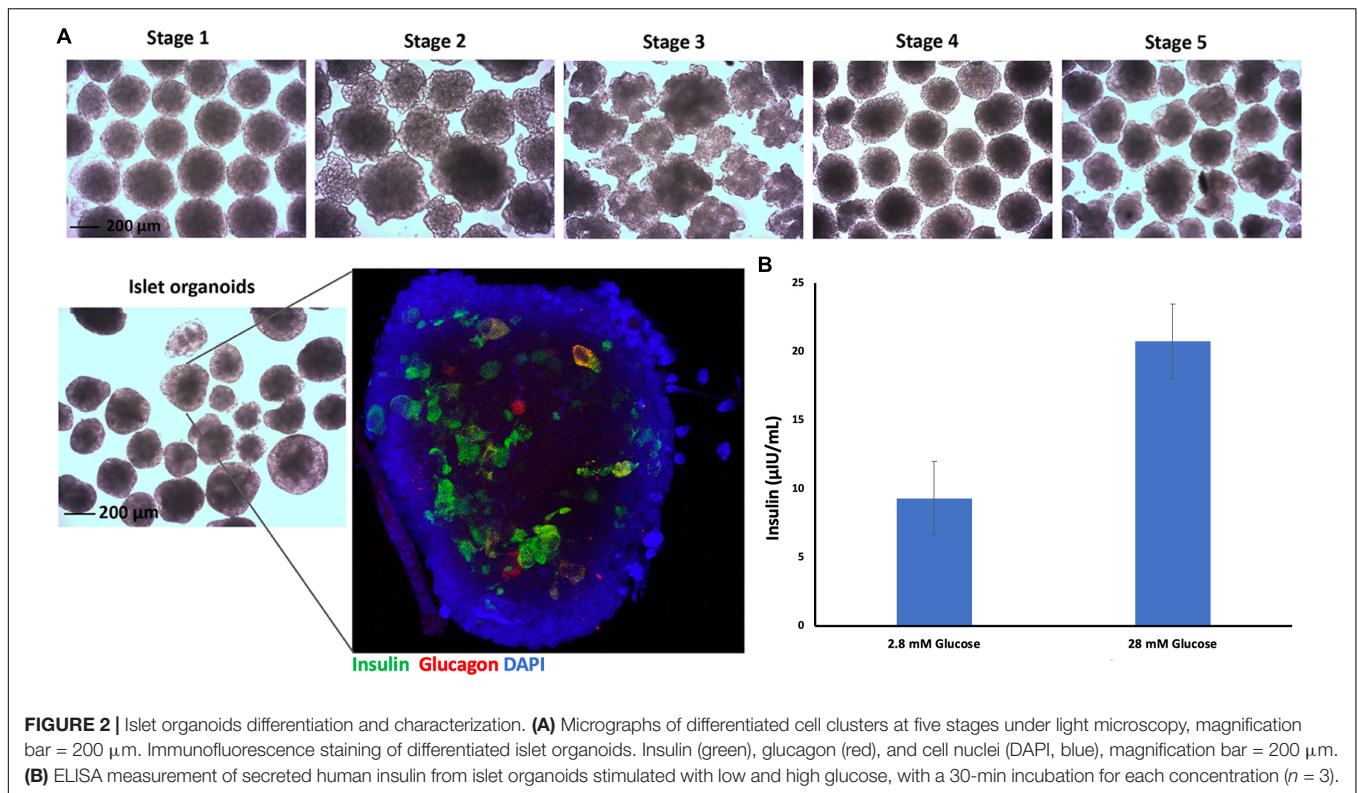
Embryoid bodies derived from hiPSC-L1 cells were produced in 3D-suspension culture to generate pancreatic islet organoids using already described protocols. After 21 days differentiated islet organoids were stained for immunofluorescence and confocal imaging to determine expression of insulin ($24 \pm 4\%$) and glucagon ($9 \pm 3\%$) in the differentiated islet organoids (Figure 2A and Supplementary Video 1). Functional test glucose-stimulated insulin secretion (GSIS) assay demonstrated the differentiated islet organoids reacted to glucose stimulation and secrete human insulin (Figure 2B). We further analyzed the expression of hormone genes in islet organoids including insulin and glucagon. Quantitative RT-PCR analysis showed high levels of insulin and glucagon gene transcripts in stage 5 cell clusters and islet organoids (Supplementary Figure 1), which was consistent with the immunofluorescence analysis.

Assessment of Labeling Efficacy and Viability of VivoTrax Labeled Islet Organoids

Nearly all of the cells within the islet organoids were labeled with VivoTrax as confirmed by anti-dextran antibody staining (Figure 3A). MTT assay showed that compared with non-labeled islet organoids, VivoTrax labeling treatment did not have significant effect on islet organoid viability (Figure 3B; $p > 0.05$). Double stained islet organoids with C-peptide (in green) and dextran showed that the VivoTrax labeled islet organoids expressed C-peptide, which demonstrated the labeling treatment did not affect insulin biosynthesis in differentiated islet organoids (Figure 3C).

Imaging of Islet Organoids Phantoms *in vitro*

In vitro MPI showed the signal intensity of phantoms increased with increasing number of islet organoids (Figure 4A). The iron content was inferred from the MPI signal by quantitative analysis of the hand-drawn ROIs of MPI intensity using VivoQuant, calibrated against a 40% fiducial marker of known iron content (2.2 μ g of iron). A linear correlation was revealed between the number of islet organoids and the MPI signal ($R^2 = 0.997$, $p < 0.0001$) (Figure 4B). In equivalent control cell populations without VivoTrax labeling, no MPI signal was detected. Likewise, ICP-OES results showed that a linear correlation was found between the number of islet organoids and the iron content ($R^2 = 0.977$, $p < 0.0001$) (Figure 4B), further confirmed the MPI quantification results.



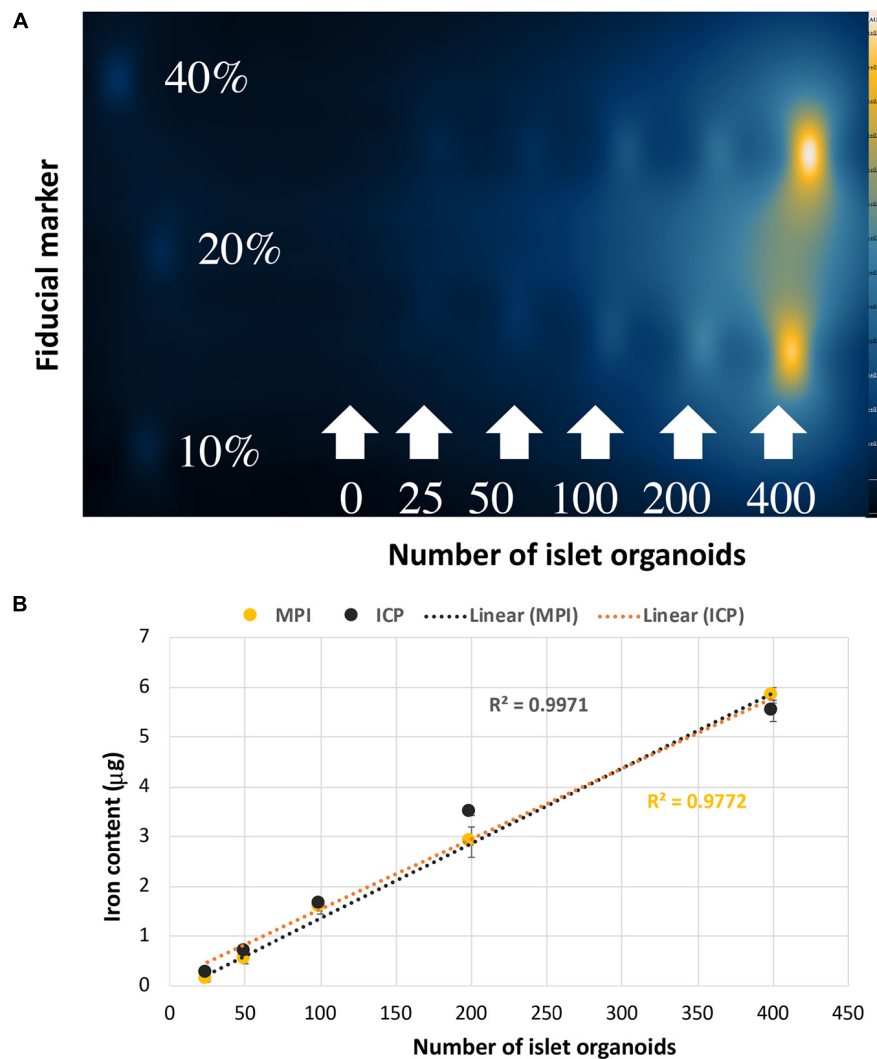


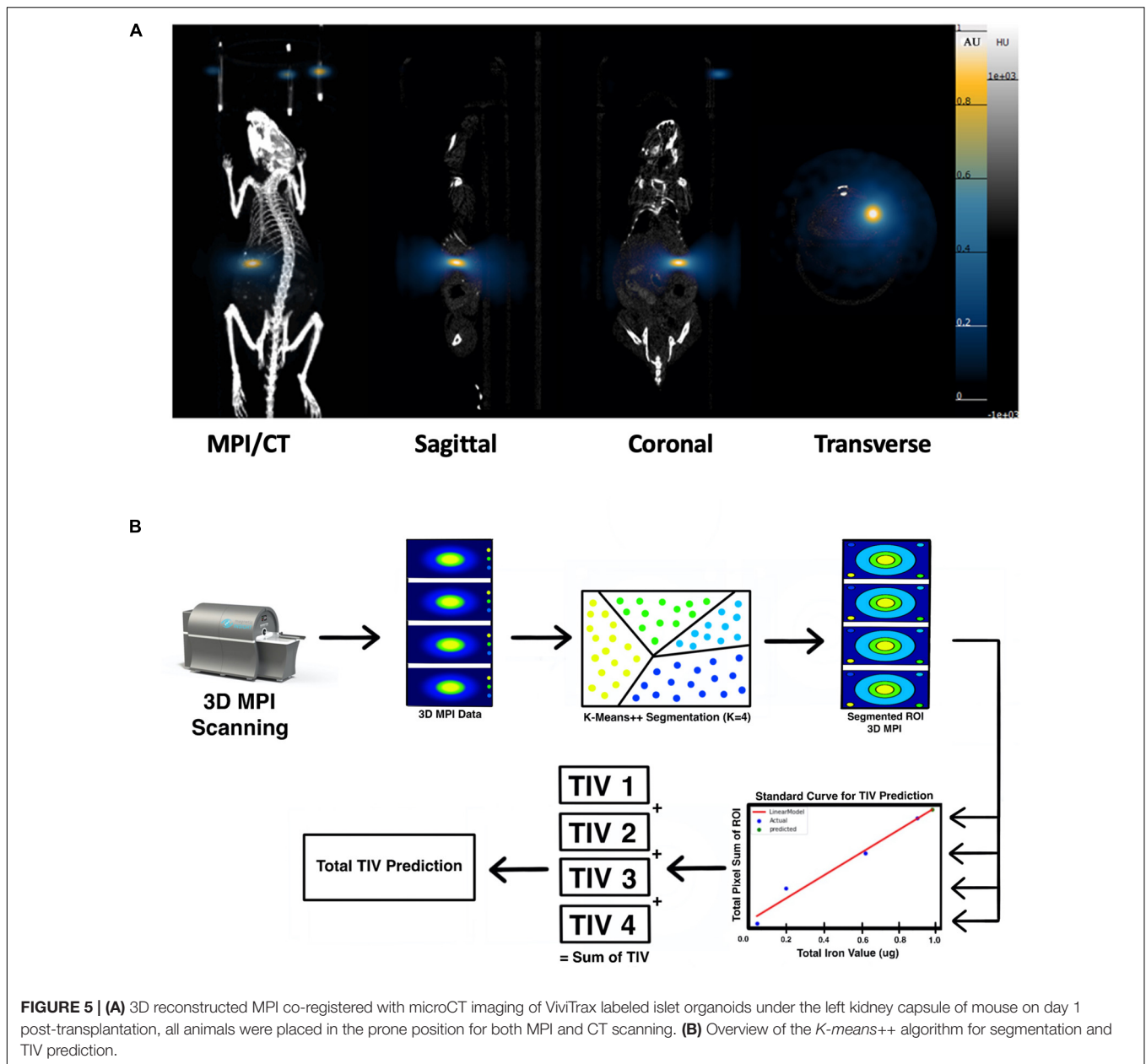
FIGURE 4 | Islet organoids phantoms imaging and iron content quantification. **(A)** MPI of the different number of SPIO labeling islet organoids phantom. **(B)** Iron content of the islet organoids phantoms measured by MPI ($R^2 = 0.9971$) and ICP-OES ($R^2 = 0.9772$) both correlated with the number of labeled islet organoids. Data are represented as mean \pm SD.

***In vivo* MPI *K-means++* Algorithm Analysis and ICC Validation**

Strong MPI signals representing labeled islet organoids were detected under the left kidney capsule from 3D images on the first day post-transplantation in all recipients (**Figure 5A** and **Supplementary Video 2**). *K-means++* algorithm was applied for the 3D segmentations and TIV estimations on the ROIs from *in vivo* MPI (**Figure 5B**). Since MPI signal is not detectable in the absence of iron oxide nanoparticles, we did not observe any signal in control animals that did not receive the labeled graft (**Supplementary Video 3**).

3D MPI were followed up at 7, and 28-day post-transplantation for these recipient mice (**Figure 6A**). **Figure 6B** depicts the output results from the single *k-means++* segmentation of the ROI from longitudinal MPI scans of mice which received islet organoid transplants. **Figure 6C** and

Supplementary Video 4 showed the 3D output of the signal *k-means++* segmentation of the ROIs from an MPI scan of a recipient mouse. As is evidenced by the eventual loss of iron over the course of 28 days, which is visible both visually and through quantification *via* TIV estimation, the algorithm is able to trace the necessary ROI from the MPI image scans of mice and predict the TIVs which portray a linear trend in correlation with increasing total pixel sum of the ROI (**Figure 6D**, $p < 0.05$). An initial increase was observed in the MPI ROI size from day 1 to 7, with a decrease in overall ROI size by day 28 (**Figures 6D,E**, $p < 0.05$). Statistical evaluation *via* two-way repeated measures ANNOVA indicated significant difference between the predicted TIV from different days. These findings are reflected in the TIV prediction of the mice from different days in which there is an increase in TIV (and ROI size) from day 1 to 7 followed by a decrease from day 7 to 28. These results were fortified by ICC



validation of the algorithm's performance in comparison to a board-certified imaging specialist. A near-excellent and excellent ICC score of 0.898 and 0.927 for single and average measures, respectively, was determined through ICC validation (Table 1, $p < 0.05$). This indicated a high degree of agreement between TIV prediction of the algorithm and the imaging specialist.

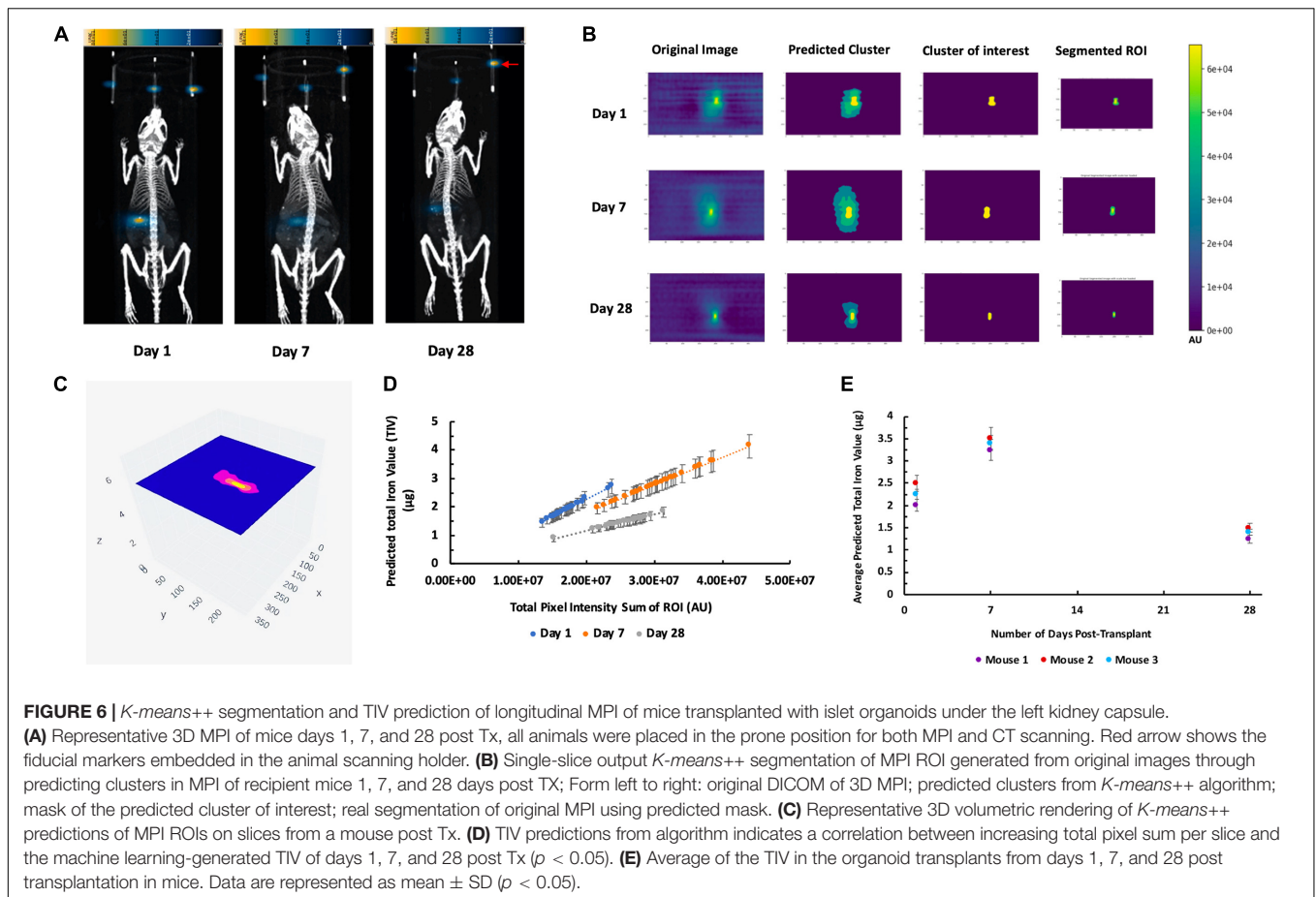
Ex vivo Immunohistochemistry

Immunofluorescence staining of the left kidney sections showed the presence of islet organoid grafts as confirmed by double staining for dextran and C-peptide 1-week post transplantation (Figure 7). Dextran expression was visible in these graft cells, which indicated that VivoTrax were retained in these transplanted cells (Figure 7). With the double immunostaining,

these graft cells also expressed C-peptide, which demonstrated insulin biosynthesis in the graft organoids (Figure 7). This *ex vivo* data, consistent with *in vivo* MPI results, attest to the feasibility of labeling islet organoids using SPIONs and monitoring these functional islet organoids by MPI after transplantation.

DISCUSSION

Stem cell replacement therapy is a promising approach for the treatment of T1D. Studies demonstrated that hiPSC can become an unlimited, relatively safe (autologous-derived cells, thus devoid of rejection risk), and an efficient alternative source to generate insulin-producing islet organoids



(Soejitno and Prayudi, 2011; Li et al., 2014; Maxwell et al., 2020). Methods to track islet organoids outcome after transplantation, however, are needed. MPI is an emerging tomographic technique that directly detects iron oxide nanoparticle tracers. These tracers are safe, non-toxic tracer, biocompatible and not normally found in the body, thus MPI images have exceptional contrast and high sensitivity. MPI imaging of these tracers provided an approach to track islet organoids and longitudinally monitor islet organoids *in vivo*. In this study, we successfully differentiated hiPSC-L1 into islet organoids and labeled islet organoids with SPIONs. Labeled islet organoids were highly effective at accumulation of SPIONs, immunostaining demonstrated nearly all of the cells within the islet organoids were labeled with SPIONs. MPI has

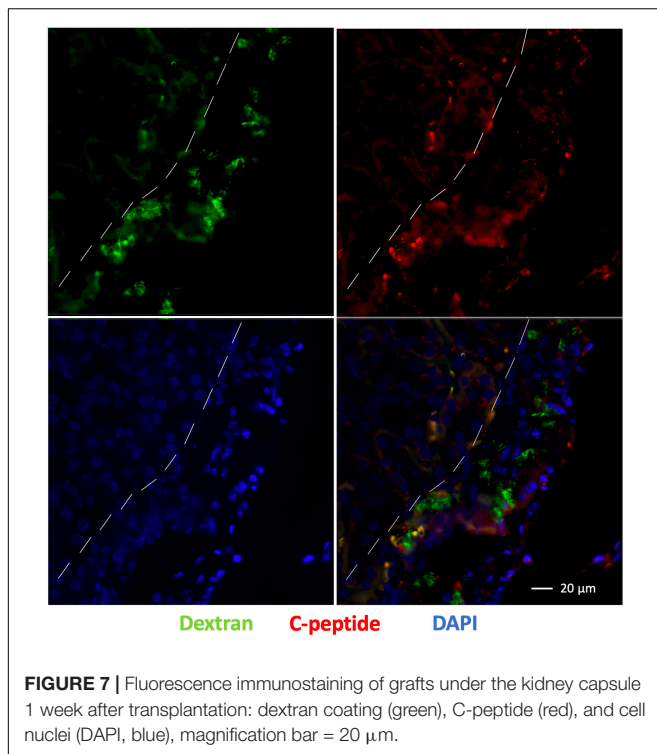
a detection sensitivity of as few as 25 islet organoids *in vitro*. The quantification demonstrates a linear correlation between MPI signal intensity and the number of labeled islet organoids. We further found that the estimated iron content from the MPI image was consistent with the iron content measured by ICP. This demonstrates that MPI is able to quantify SPIONs-labeled islet organoids *in vitro*, which provides evidence that MPI may be able to track and quantify islet organoids *in vivo*. We used 800 labeled islet organoids per transplant to establish the feasibility of MPI detection *in vivo*. MPI 3D images with a co-registered CT show strong signals were detected under the left kidney capsule on the first day in all recipients that represented labeled islet organoids.

TABLE 1 | Intraclass correlation coefficient (ICC) validation of ROI segmentation and TIV prediction of the *K-means++* based algorithm in comparison to an imaging specialist.

Type	Interclass correlation	95% Confidence interval: lower bound	95% Confidence interval: upper bound	F-test with true value 0: df	F-test with true value 0: sig.
Single measures	0.898	0.621	0.979	14	0.001
Average measures	0.927	0.546	0.973	14	0.001

Top row: data for single measures.

Bottom row: data for average measures.



To monitor reproducibly the transplanted islet organoids longitudinally and analyze the ROIs from the MPI scans of mice, the canonical unsupervised ML algorithm of *k-means++* was employed in conjunction with a linear regression based standard curve model. This algorithm is different from that which we applied previously to 2D MPI scans of transplanted islets, because it applies the algorithm to multiple layers of a 3D MPI scan (Hayat et al., 2020). This signal is indicative of the current nanoparticle content inside the mice which is evidence of the islet organoid cell content at the time of MPI scanning. Through segmentation and TIV prediction on the MPI data of the mice from days 1, 7, and 28, the algorithm was able to monitor the transplanted islet organoids longitudinally with indications on total iron content within subjects in a 3D manner.

The reasons why we chose VivoTrax for this study was because this tracer has been widely used for MPI. There are other SPIONs available, Feraheme (ferumoxytol) is another SPIONs product that is clinically used for iron anemia/deficiency and may have potential for MPI, although likely with less sensitivity due to its smaller size (Bulte, 2019). It was unexpected that there would be an increase in TIV (and ROI size) of the labeled transplants from day 1 to 7. The possible explanations for this finding include environmental induced degradation of the dextran coating of the VivoTrax, which may increase the total signal intensity, decreasing the peak signal intensity. Dynamic light scattering (DLS) studies have demonstrated that an increase in the nanoparticle size of degraded VivoTrax from 75 to 330 nm, which suggests the removal of the dextran coating resulted aggregation of the nanocrystal core *in vitro* (Guzy et al., 2020). Another factor that may contribute to this signal increase

could be cell division triggered aggregation and releasing of the iron oxides nanostructure from encapsulated VivoTrax in the proliferating stem cell differentiated islet organoids. Possible explanation for the increase in TIV and ROI size might also be in relation with restructuration of the graft upon transplantation: the cell cluster break down and migrate to occupy the space under the kidney capsule, allowing vascularization and innervation of the grafts. Davalli et al. (1996) investigated syngeneic islets transplantation under the kidney capsule in a murine model. Grafts were harvested 1, 3, 7, and 14 days after transplantation and analyzed for morphology and insulin content. Their results showed that substantial damage in islet grafts was found on days 1 and 3 with apoptotic nuclei and necrotic cores; Tissue remodeling occurred with stable graft appearance on day 14; Graft insulin content decreased on day 1 and fell even further on days 3 and 7. We do agree that there are differences between *in vivo* imaging and histological evaluations, hence, we want to emphasize this is the first study on MPI of stem cell differentiated islet organoids transplantation, which is similar but still different from islet transplantation. In addition, measurement of labeled islet organoids in our study relies on imaging of the aforementioned nanoparticles, whereas Davalli et al. (1996) evaluated and quantified graft loss based on factors such as *ex vivo* morphology and insulin content/mRNA expression. This initial observation, irrespective of underlying mechanism, demonstrates the power of our data analysis algorithm for *in vivo* MPI.

Our method faces limitations as it cannot be applied to MPI scans that do not have the reference fiducial markers in the proper spatial orientation. Furthermore, it only takes into account three concentrations of fiducial markers in order to generate the standard curve with which the TIV is predicted. Future studies involving deep learning can potentially resolve these limitations by training on known TIV of diverse phantoms and their associated ICP values in order to predict the unknown TIV of a new ROI (Hayat and Wang, 2020). Nonetheless, the current algorithm provides a standardized, automated method for TIV analysis of transplanted organoids *in vivo*. This has implications for future studies in which the therapeutic effect of the transplanted islet organoids can be observed in diabetic mice, and such ML algorithms will be employed to accurately monitor the labeled iron signals from the organoid cell clusters longitudinally. This also has other implications in applying AI to monitor different cell-based therapies such as pancreatic islet transplantation, chimeric antigen receptor (CAR), T-Cell therapy, and other cellular approaches to treating diseases.

CONCLUSION

In this study, we demonstrated the feasibility of longitudinal *in vivo* tracking and quantifying implanted islet organoids grafts for 28 days using MPI and ML algorithm. We believe that MPI could play an important role in monitoring the grafts, by directly imaging of the graft itself. In future studies, we plan to transplant islet organoids in a diabetic mouse model and verify and improve the *K-mean++* algorithm for unbiased quantification of *in vivo* MPI.

DATA AVAILABILITY STATEMENT

The original contributions presented in the study are included in the article/**Supplementary Material**, further inquiries can be directed to the corresponding author/s.

ETHICS STATEMENT

The animal study was reviewed and approved by Institutional Animal Care and Use Committee (IACUC) at the Michigan State University.

AUTHOR CONTRIBUTIONS

AS, HH, SL, JB, BD, MG, NT, and JD researched the data. HH and AS led the data analysis. ET, JB, BD, MG, and JG participated in data analysis. AS, HH, WL, AAI, and AAG participated in drafting the manuscript. PW conceived the idea, designed the study, drafted the manuscript and is the guarantor of this work and, as such, had full access to all the data in the study and take responsibility for the integrity of the data and the accuracy of the data analysis. All authors contributed to the article and approved the submitted version.

REFERENCES

- Bulte, J. W., Walczak, P., Gleich, B., Weizenecker, J., Markov, D. E., Aerts, H. C., et al. (2011). MPI Cell Tracking: what Can We Learn from MRI? *Proc. SPIE Int. Soc. Opt. Eng.* 7965:79650z. doi: 10.1117/12.879844
- Bulte, J. W. M. (2019). Superparamagnetic iron oxides as MPI tracers: a primer and review of early applications. *Adv. Drug Deliv. Rev.* 138, 293–301. doi: 10.1016/j.addr.2018.12.007
- Bulte, J. W. M., and Daldrup-Link, H. E. (2018). Clinical Tracking of Cell Transfer and Cell Transplantation: trials and Tribulations. *Radiology* 289, 604–615. doi: 10.1148/radiol.2018180449
- Crabbe, A., Vandeputte, C., Dresselaers, T., Sacido, A. A., Verdugo, J. M., Eyckmans, J., et al. (2010). Effects of MRI contrast agents on the stem cell phenotype. *Cell Transplant* 19, 919–936. doi: 10.3727/096368910X494623
- Davalli, A. M., Scaglia, L., Zangen, D. H., Hollister, J., Bonner-Weir, S., and Weir, G. C. (1996). Vulnerability of islets in the immediate posttransplantation period: Dynamic changes in structure and function. *Diabetes* 45, 1161–1167. doi: 10.2337/diab.45.9.1161
- Guzy, J., Chakravarty, S., Buchanan, F., Chen, H., Gaudet, J., Hix, J., et al. (2020). Complex Relationship between Iron Oxide Nanoparticle Degradation and the Signal Intensity in Magnetic Particle Imaging. *ACS Appl. Nano Mater.* 3, 3991–3999. doi: 10.1021/acsnm.0c00779
- Hayat, H., Sun, A., Hayat, H., Liu, S., Talebloo, N., Pinger, C., et al. (2020). Artificial Intelligence Analysis of Magnetic Particle Imaging for Islet Transplantation in a Mouse Model. *Mol. Imaging Biol.* 23, 18–29. doi: 10.1007/s11307-020-01533-5
- Hayat, H., and Wang, P. (2020). The application of artificial intelligence in biomedical imaging. *Am. J. Biomed. Sci. Res.* 8, 228–231. doi: 10.34297/ajbsr.2020.08.001279
- Janowski, M., Walczak, P., Kropiwnicki, T., Jurkiewicz, E., Domanska-Janik, K., Bulte, J. W., et al. (2014). Long-term MRI cell tracking after intraventricular delivery in a patient with global cerebral ischemia and prospects for magnetic navigation of stem cells within the CSF. *PLoS One* 9:e97631. doi: 10.1371/journal.pone.0097631
- Khandhar, A. P., Keselman, P., Kemp, S. J., Ferguson, R. M., Goodwill, P. W., Conolly, S. M., et al. (2017). Evaluation of PEG-coated iron oxide nanoparticles

FUNDING

The project was partly funded by the 1R03EB028349 from NIH/NIBIB to PW.

ACKNOWLEDGMENTS

We would like to thank L. Karl Olson (Department of Physiology, College of Natural Science, Michigan State University), Ripla Arora (The Institute for Quantitative Health Science and Engineering, Department of Obstetrics, Gynecology and Reproductive Biology, College of Human Medicine, Michigan State University), Christopher H. Contag (The Institute for Quantitative Health Science and Engineering, Department of Biomedical Engineering, College of Engineering, Michigan State University), and Anna Moore (Precision Health Program, Michigan State University) for their great discussions and support.

SUPPLEMENTARY MATERIAL

The Supplementary Material for this article can be found online at: <https://www.frontiersin.org/articles/10.3389/fcell.2021.704483/full#supplementary-material>

- as blood pool tracers for preclinical magnetic particle imaging. *Nanoscale* 9, 1299–1306. doi: 10.1039/c6nr08468k
- Li, J., Song, W., Pan, G., and Zhou, J. (2014). Advances in understanding the cell types and approaches used for generating induced pluripotent stem cells. *J. Hematol. Oncol.* 7:50. doi: 10.1186/s13045-014-0050-z
- Magnitsky, S., Zhang, J., Idiyatullin, D., Mohan, G., Garwood, M., Lane, N. E., et al. (2017). Positive contrast from cells labeled with iron oxide nanoparticles: quantitation of imaging data. *Magn. Reson. Med.* 78, 1900–1910. doi: 10.1002/mrm.26585
- Makela, A. V., Gaudet, J. M., Schott, M. A., Sehl, O. C., Contag, C. H., and Foster, P. J. (2020). Magnetic Particle Imaging of Macrophages Associated with Cancer: filling the Voids Left by Iron-Based Magnetic Resonance Imaging. *Mol. Imaging Biol.* 22, 958–968. doi: 10.1007/s11307-020-01473-0
- Maxwell, K. G., Augsornworawat, P., Velazco-Cruz, L., Kim, M. H., Asada, R., Hogrebe, N. J., et al. (2020). Gene-edited human stem cell-derived beta cells from a patient with monogenic diabetes reverse preexisting diabetes in mice. *Sci. Transl. Med.* 12, eaax9106. doi: 10.1126/scitranslmed.aax9106
- Pomposelli, T., Wang, P., Takeuchi, K., Miyake, K., Ariyoshi, Y., Watanabe, H., et al. (2020). Protection of Pancreatic Islets Using Theranostic Silencing Nanoparticles in a Baboon Model of Islet Transplantation. *Diabetes* 69, 2414–2422. doi: 10.2337/db20-0517
- Rizzo, S., Petrella, F., Politi, L. S., and Wang, P. (2017). Molecular Imaging of Stem Cells: in Vivo Tracking and Clinical Translation. *Stem Cells Int.* 2017:1783841. doi: 10.1155/2017/1783841
- Russ, H. A., Parent, A. V., Ringler, J. J., Hennings, T. G., Nair, G. G., Shveygert, M., et al. (2015). Controlled induction of human pancreatic progenitors produces functional beta-like cells in vitro. *EMBO J.* 34, 1759–1772. doi: 10.15252/embj.201591058
- Soejitno, A., and Prayudi, P. K. (2011). The prospect of induced pluripotent stem cells for diabetes mellitus treatment. *Ther. Adv. Endocrinol. Metab.* 2, 197–210. doi: 10.1177/2042018811420198
- Talebloo, N., Gudi, M., Robertson, N., and Wang, P. (2020). Magnetic Particle Imaging: current Applications in Biomedical Research. *J. Magn. Reson. Imaging* 51, 1659–1668. doi: 10.1002/jmri.26875

- Wang, L., Song, Y., Parikh, A., Joyce, P., Chung, R., Liu, L., et al. (2019). Doxorubicin-Loaded Delta Inulin Conjugates for Controlled and Targeted Drug Delivery: development, Characterization, and In Vitro Evaluation. *Pharmaceutics* 11:581. doi: 10.3390/pharmaceutics11110581
- Wang, P., and Aguirre, A. (2018). New Strategies and In Vivo Monitoring Methods for Stem Cell-Based Anticancer Therapies. *Stem Cells Int.* 2018:7315218. doi: 10.1155/2018/7315218
- Wang, P., Goodwill, P. W., Pandit, P., Gaudet, J., Ross, A., Wang, J., et al. (2018). Magnetic particle imaging of islet transplantation in the liver and under the kidney capsule in mouse models. *Quant. Imaging Med. Surg.* 8, 114–122. doi: 10.21037/qims.2018.02.06
- Wang, P., Liu, Q., Zhao, H., Bishop, J. O., Zhou, G., Olson, L. K., et al. (2020). miR-216a-targeting theranostic nanoparticles promote proliferation of insulin-secreting cells in type 1 diabetes animal model. *Sci. Rep.* 10:5302. doi: 10.1038/s41598-020-62269-4
- Wang, P., and Moore, A. (2012). Molecular imaging of stem cell transplantation for neurodegenerative diseases. *Curr. Pharm. Des.* 18, 4426–4440. doi: 10.2174/138161212802481255
- Wang, P., Yigit, M. V., Medarova, Z., Wei, L., Dai, G., Schuetz, C., et al. (2011). Combined small interfering RNA therapy and in vivo magnetic resonance imaging in islet transplantation. *Diabetes* 60, 565–571. doi: 10.2337/db10-1400
- Wang, P., Yigit, M. V., Ran, C., Ross, A., Wei, L., Dai, G., et al. (2012). A theranostic small interfering RNA nanoprobe protects pancreatic islet grafts from adoptively transferred immune rejection. *Diabetes* 61, 3247–3254. doi: 10.2337/db12-0441
- Wu, L. C., Zhang, Y., Steinberg, G., Qu, H., Huang, S., Cheng, M., et al. (2019). A Review of Magnetic Particle Imaging and Perspectives on Neuroimaging. *AJNR Am. J. Neuroradiol.* 40, 206–212. doi: 10.3174/ajnr.A5896
- Yu, E. Y., Bishop, M., Zheng, B., Ferguson, R. M., Khandhar, A. P., Kemp, S. J., et al. (2017). Magnetic Particle Imaging: a Novel in Vivo Imaging Platform for Cancer Detection. *Nano Lett.* 17, 1648–1654. doi: 10.1021/acs.nanolett.6b04865
- Zheng, B., Vazin, T., Goodwill, P. W., Conway, A., Verma, A., Saritas, E. U., et al. (2015). Magnetic Particle Imaging tracks the long-term fate of in vivo neural cell implants with high image contrast. *Sci. Rep.* 5:14055. doi: 10.1038/srep14055
- Zheng, B., von See, M. P., Yu, E., Gunel, B., Lu, K., Vazin, T., et al. (2016). Quantitative Magnetic Particle Imaging Monitors the Transplantation, Biodistribution, and Clearance of Stem Cells In Vivo. *Theranostics* 6, 291–301. doi: 10.7150/thno.13728

Conflict of Interest: JG was employed by company Magnetic Insight Inc.

The remaining authors declare that the research was conducted in the absence of any commercial or financial relationships that could be construed as a potential conflict of interest.

The reviewer RS declared a shared affiliation with the authors to the handling editor at the time of review.

Publisher's Note: All claims expressed in this article are solely those of the authors and do not necessarily represent those of their affiliated organizations, or those of the publisher, the editors and the reviewers. Any product that may be evaluated in this article, or claim that may be made by its manufacturer, is not guaranteed or endorsed by the publisher.

Copyright © 2021 Sun, Hayat, Liu, Tull, Bishop, Dwan, Gudi, Talebloo, Dizon, Li, Gaudet, Alessio, Aguirre and Wang. This is an open-access article distributed under the terms of the Creative Commons Attribution License (CC BY). The use, distribution or reproduction in other forums is permitted, provided the original author(s) and the copyright owner(s) are credited and that the original publication in this journal is cited, in accordance with accepted academic practice. No use, distribution or reproduction is permitted which does not comply with these terms.